Frontiers of Information Technology & Electronic Engineering
www.jzus.zju.edu.cn; engineering.cae.cn; www.springerlink.com
ISSN 2095-9184 (print); ISSN 2095-9230 (online)
E-mail: jzus@zju.edu.cn

Enhancing modelling accuracy of cascaded spline adaptive filters using the remora optimisation algorithm: application to real-time systems

Lakshminarayana JANJANAM‡[1], Suman Kumar SAHA[2], Rajib KAR[3]

[1]*Department of ECE, Sasi Institute of Technology & Engineering, Tadepalligudem, Andhra Pradesh, 534101, India*

[2]*Department of ECE, National Institute of Technology, Raipur, Chhattisgarh, 492010, India*

[3]*Department of ECE, National Institute of Technology Durgapur, West Bengal, 713209, India*

E-mail: jlphd.nitrr@gmail.com; namus.ahas@gmail.com; rajibkarece@gmail.com

Received Dec. 3, 2023; Revision accepted Mar. 20, 2024; Crosschecked

Unedited

Abstract: In this paper we first introduce a new approach to optimise the cascaded spline adaptive filter (CSAF) for identifying unknown nonlinear systems by using a meta-heuristic optimisation algorithm (MOA). The CSAF architecture combines Hammerstein and Wiener systems, where the nonlinear blocks are implemented with the spline network. The algorithms used optimise the weights of the spline interpolation function and linear filter by using an adequately weighted cost function, leading to improved filter stability, steady state performance, and guaranteed convergence to globally optimal solutions. In this study we investigated two CSAF architectures: Hammerstein-Wiener SAF (HW-SAF) and Wiener-Hammerstein SAF (WH-SAF) structures. These architectures have been designed using gradient-based approaches which are inefficient due to poor convergence speed, and produce suboptimal solutions in a Gaussian noise environment. To avert these difficulties, we estimated the design parameters of CSAF architecture using four independent MOAs: differential evolution (DE), brain storm optimisation (BSO), multi-verse optimiser (MVO) and a recently proposed remora optimisation algorithm (ROA). In ROA, the remora factor's control parameters produce near-global optimal parameters with a faster convergence speed. ROA also ensures the most passably balanced exploration and exploitation phases compared to DE, GSA and SSA-based design approaches. Finally, the identification results of three numerical and industry-specific benchmark systems, including coupled electric drives, a thermic wall and a continuous stirred tank reactor, are presented to emphasise the effectiveness of the ROA-based CSAF design.

Key words: Cascade spline adaptive filter; Nonlinear system identification; Remora optimisation algorithm
https://doi.org/10.1631/FITEE.2300817 **CLC number:**

1 Introduction

The adaptive filtering technique is extensively applied to solve various engineering problems in the signal processing field, such as active noise control (Raja et al., 2018), system identification (Zhang et al., 2021), channel estimation and equalisation (Zhang et al., 2021), noise cancellation (Yadav et al., 2022), and echo cancellation (Sankar et al., 2020). The use of the technique is well-established for system identification problems due to its versatility in many design-oriented accurate word problems. The primary linear adaptive filter performs better if the plant exhibits linear characteristics, producing unacceptable results (Janjanam et al., 2021b). In general, real systems are nonlinear. Hence, designing a nonlinear system to handle such nonlinearity is essential. Many identification models for nonlinear plant identification (Janjanam et al., 2021b) are described below.

The Volterra filter (Wang et al., 2022; Janjanam et al., 2021a) and its improved variant, the kernel adaptive filter (KAF) (Garcia-Vega et al., 2020), are

‡ Corresponding author
ORCID: Lakshminarayana JANJANAM, https://orcid.org/0000-0001-5340-4058
© Zhejiang University Press 2024

nonlinear filters that are widely used to characterise any nonlinearity theoretically. However, their computational complexity (CC) is too high and requires many parameters. Although the neural network (NN) (Li et al., 2017; Chen et al., 2022) is simple and flexible to design the problem, it has high CC and quickly becomes trapped in local optimal solutions. The functional link artificial neural network (FLANN) (Patel et al., 2016) is another efficient model for nonlinear plant modelling that has the structure of a higher order Volterra series with less CC. However, the identification accuracy and CC of the FLANN depend on the nature of the function used for input signal expansion.

Chaudhary et al. (2019) noted that different kinds of block-oriented models (BOMs) are used to represent nonlinear systems, especially industry-specific plants. A BOM consists of a combination of linear dynamic filters and nonlinear static functions. The primary classes of BOMs are Hammerstein and Wiener models. The series connection of a nonlinear function and linear filter form the structure of the Hammerstein model (Chaudhary et al., 2019; Janjanam et al., 2022a; Mehmood et al., 2019a; Mehmood et al., 2019b). Janjanam et al. (2022a) identified various Hammerstein benchmark plants using the social mimic optimisation algorithm-assisted Kalman filter, and successfully estimated the state of the heating system and cascade tanks. Moreover, Mehmood et al, (2019a and 2019b) enforced the backtracking search optimisation algorithm for Hammerstein model tracking (Mehmood et al., 2019a) and modelled the electrical muscle system based on Hammerstein (Mehmood et al., 2019b).

In contrast, a Wiener model is formed by a cascading linear filter that is succeeded by a nonlinear function (Pal et al., 2017; Janjanam et al., 2022b). Various evolutionary techniques, namely brainstorm optimisation (Pal et al., 2017) and moth-flame optimisation (Janjanam et al., 2022b) algorithms, are used for the tracking of standard Wiener system outputs and produce better results than other reported methods (Janjanam et al., 2022b). MOAs can also solve highly complex and multidisciplinary problems. Jia et al. (2023) proposed a crayfish optimisation algorithm and used it to optimise complex CEC2014 benchmark test functions and solve design problems of various practical systems, such as a tension/compression spring, welded beam, and pressure vessel. Dynamic Harris Hawks optimisation with a mutation algorithm (Jia et al., 2019) was successfully used for segmentation of satellite images. Xu et al. (2019) successfully used a hybrid dragonfly algorithm and differential evolution algorithms for multilevel colour image segmentation. The above discussion confirms that MOAs can be used to efficiently identify complex and multi-dimensional systems and derive near-global optimal coefficients with a high convergence speed compared to other approaches. Hence, we used MOA in this study to estimate CSAFs.

Unfortunately, Hammerstein and Wiener models individually do not guarantee good identification results for practical design-oriented problems (Li and Ren 2018). Hence, a cascade of the above models is used. In earlier studies (Li and Ren 2018; Janjanam et al., 2022c), the outputs of a turntable servo system (Li and Ren 2018) and real-time nonlinear electronic system (Janjanam et al., 2022c) were effectively tracked using one of the most popular cascaded architectures, called the Wiener-Hammerstein (WH) model. The WH model gives the best results in the presence of noise (Liu et al., 2021; Esmaeilani et al., 2021). In practical plants, namely the ball-and-beam and robot arm systems, Janjanam et al. (2022d) used an optimally tuned Sage-Husa adaptive Kalman filter based on another cascaded structure called Hammerstein-Wiener (HW).

Recently, the parameters of various highly non-linearity-oriented HW plants were identified using Levenberg-Marquardt (Hammar et al., 2019) and weighted differential evolution (Mehmood et al., 2022) algorithms. However, the methods proposed for cascade model identification (Li and Ren 2018; Esmaeilani et al., 2021; Janjanam et al., 2022d; Hammar et al., 2019) were improved versions of gradient-based approaches characterised by low convergence speed and moderate estimation accuracy. Moreover, very few studies (Janjanam et al., 2022c; Janjanam et al., 2022d; Mehmood et al., 2022) have used MOA-based methods. Hence, in this study, we focused only on a cascaded model with efficient MOAs. In addition, the tracking accuracy of HW and WH models depends on the type of nonlinearity used in the nonlinear function blocks (Li and Ren 2018). Recent studies (Scarpiniti et al., 2014; Gao et al., 2023) have confirmed that spline nonlinearity gives

Unedited

better identification accuracy than other nonlinearities such as polynomials and piece-wise linear functions.

Spline adaptive filters (SAFs) have recently attracted increasing attention because of their higher performance accuracy, simplicity and flexibility in implementation, and lower CC. They have been used in numerous applications such as unknown system modelling (Scarpiniti et al., 2014), nonlinear active noise control (Gao et al., 2023), and channel estimation in wireless sensor network applications (Mishra et al., 2023). A series of intriguing studies on SAFs for nonlinear system identification has been published. Scarpiniti et al. have developed various SAF architectures such as Hammerstein SAF (HSAF) (Scarpiniti et al., 2014), Wiener SAF (WSAF) (Scarpiniti et al., 2013; Scarpiniti et al., 2015a), and cascaded SAFs (HW-SAF and WH-SAF) (Scarpiniti et al., 2015b; Scarpiniti et al., 2018) based on the least mean square (LMS) algorithm for effective modelling of nonlinear plants. Moreover, the robustness of these SAFs has been investigated under different signal-to-noise ratio (SNR) conditions. Yang et al. (2019) and Yu et al. (2021) proposed other unique cost functions and modified stochastic gradient techniques to improve the robustness of SAF against noises.

To reduce the effect of impulse noise, researchers have designed SAFs using different techniques such as the generalised maximum versoria criterion algorithm (GMVC) (Guo and Zhi 2022), Heaviside step function (Guan et al., 2022) and arctangent-exponential hyperbolic cosine (Guo et al., 2022). In addition, Liu and Zhao (2023) proposed a complex valued SAF based on a two-dimensional look-up table, yielding good estimation results with low CC. Li et al., (2023) have developed a frequency domain SAF based on a half-quadratic criterion (HQC), offering better robustness and CC. Guan and Biswal (2023) proposed SAF-Adagrad and SAF-RMSProp methods to improve convergence and steady-state performance in nonlinear system modelling.

Recently, Gao et al. (2024) developed a q-gradient LMS with a variable step size algorithm for the design of SAF. This technique further balances the convergence rate and steady-state error and solves deficiency due to constant step size. Yu et al. (2024) effectively designed a robust sub-band HSAF with exponential, hyperbolic cosine fitness functions and used it to solve system identification and acoustic echo cancellation problems. However, the SAFs mentioned above were modelled with stochastic gradient approaches, which easily traverse to locally optimal solutions and take a considerable number of epochs (the order of 104) to converge, and the accuracy of results depends on the initial parameters settings. Moreover, existing techniques have been developed based on some prior assumptions, leading to algorithm complexity and producing low-quality solutions when dealing with a higher data rate and practical systems (Scarpiniti et al., 2015b; Scarpiniti et al., 2018). MOA is the only solution considered here to address these problems.

Janjanam et al., (2023) have proposed a novel methodology to solve the design problem of HSAF using MOA. They proposed an efficient cost function minimised with the snake optimiser algorithm (SOA) by simultaneously amending the design parameters of HSAF, such as the linear filter coefficients and the weights of spline control points. Their experimental results confirmed that the MOA-based design approach derives the global optimal HSAF coefficients and improves the filter convergence speed and performance stability compared with previous methods (Janjanam et al., 2023). Based on the knowledge gained from their study, in this article, we present two distinct CSAFs (HW-SAF and WH-SAF) successfully designed for nonlinear system modelling using an efficient MOA called ROA.

The main contributions of this article are as follows:

i.We introduce the novel application of MOAs through ROA, MVO, BSO and DE algorithms for the reliable, accurate and robust estimation of CSAF nonlinear systems (WH-SAF and HW-SAF). Moreover, we analyse their performance by varying the noise level from low to high.

ii.The outcomes of several independent tests are analysed to estimate the stability of the methodology.

iii. Holm's hypothesis test is applied to compare the consistency of the proposed ROA-based design with that of other designs.

iv. The estimation accuracy of the proposed scheme is verified with mean absolute error (MAE), root mean squared deviation (RMSD), mean weight deviation (MWD) and Thiel's inequality coefficient (TIC) metrics.

iv. The potency of the WH-SAF and HW-SAF models over other most familiar identification models for nonlinear system design is explored and the com-

Unedited

plexity (CC) of the proposed method is discussed.
v.The identification problem of three real-life benchmark systems is examined.

The rest of the paper is organised as follows. The measurement model of both the HW-SAF and WH-SAF architectures and cost functions are presented in Section 2. Section 3 provides the identification steps of the CSAF system using the proposed ROA-based technique. Section 4 presents the results from simulation of various numerical and real-world problems. Finally, some conclusions and suggestions for further work on CSAF design are given in Section 5.

2 Problem description

SAF's basic theory and working principles are available in Scarpiniti et al. (2013) and Scarpiniti et al. (2014). In this section, we derive the measurement forms and cost functions of the chosen models.

2.1. Mathematical modelling of HW-SAF and its cost function formulation

A schematic diagram of an HW-SAF is shown in Fig. 1, where a linear filter (LF) is sandwiched between two memoryless nonlinear static functions, which are implemented with the SAF architecture (Scarpiniti et al., 2015b). The NSAF structure consists of a nonlinear network of adaptable LUT and a spline interpolator. Fig. 1 shows that at time instant n, the signals $u[n]$ and $y[n]$ are the system's input and output, respectively. The symbols of NSAF-1 and NSAF-2 blocks are separately denoted by superscripts 1 and 2.

Step 1: Mathematical modelling of NSAF-1

The nonlinear relationship between the signals $u[n]$ and $g[n]$ of NSAF-1 is expressed as $g[n]=f^{(1)}(u[n],r_{i,n}^{(1)})$ (Scarpiniti et al., 2015b), where $f^{(1)}$ denotes the nonlinear spline function of NSAF-1, which is a smooth parameter curve interpolated by the definite length of control points in the LUT, and the variable $r_{i,n}^{(1)}$ is the spline control point vector represented by $r_{i,n}^{(1)}\in\Re^{4\times 1}=[r_{i,n}^{(1)},r_{i+1,n}^{(1)},r_{i+2,n}^{(1)},r_{i+3,n}^{(1)}]^T$, where the symbols $\Re$ and T denote the actual value and vector transpose, respectively. The spline estimation is based on the local parameter (ρ) and span index (i). The calculation of these two parameters for the NSAF-1 at time instant n is given as (Scarpiniti et al., 2015b):

$$i_n^{(1)}=\lfloor u[n]/\Delta u^{(1)}\rfloor+(R^{(1)}-1)/2;$$
$$\rho_n^{(1)}=u[n]/\Delta u^{(1)}-\lfloor u[n]/\Delta u^{(1)}\rfloor \tag{1}$$

where $\Delta u^{(1)}$ is the sampling interval between the control points, $\lfloor\bullet\rfloor$ is the floor operator and $R^{(1)}$ denotes the total number of control points.

The response $g[n]$ of the NSAF-1 block for the input $u[n]$ is mathematically expressed as

$$g[n]=\rho_{i,n}^{(1)T}Cr_{i,n}^{(1)} \tag{2}$$

where $\rho_{i,n}^{(1)}\in\Re^{4\times 1}=[\rho_{i,n}^{3(1)},\rho_{i,n}^{2(1)},\rho_{i,n}^{(1)},1]^T$ and the pre-measured 4×4 spline basis matrix C is either B-spline (C_B) or Catmull–Rom (CR) spline (C_{CR}) (Scarpiniti et al., 2013) as given in Eq. (3).

$$C_B=\frac{1}{6}\begin{bmatrix}-1&3&-3&1\\3&-6&3&0\\-3&0&3&0\\1&4&1&0\end{bmatrix},\ C_{CR}=\frac{1}{2}\begin{bmatrix}-1&3&-3&1\\2&-5&4&-1\\-1&0&1&0\\0&2&0&0\end{bmatrix} \tag{3}$$

Step 2: Mathematical modelling of linear filter

The output $q[n]$ of the LF (finite impulse response (FIR) filter) block, as shown in Fig. 1, is expressed as $q[n]=h_n^T g_n$, where $h_n\in\Re^{N\times 1}=[h[0],h[1],...,h(N-1)]^T$ is the weight vector of the adaptive LF of length N and the signal vector, $g_n=[g[n],g[n-1],...,g[n-N+1]]^T$, where $g[n]$ is the output of the NSAF-1, as given in Eq. (2).

Step 3: Mathematical modelling of NSAF-2

The output $q[n]$ of the LF block is the input to the NSAF-2 block (Fig. 1). Like NSAF-1, the relationship between the input $q[n]$ and output $y[n]$ of NSAF-2 is expressed as $y[n]=f^{(2)}(q[n],r_{i,n}^{(2)})$ (Scarpiniti et al., 2015b), where $f^{(2)}$ and $r_{i,n}^{(2)}$ denote the nonlinear spline function and spline control point vector of NSAF-2, respectively. $r_{i,n}^{(2)}$ is represented

Unedited

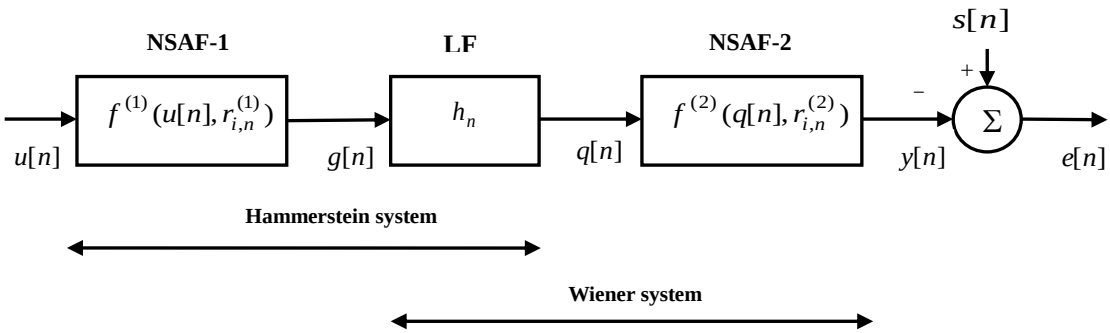

Fig. 1. Schematic diagram of an HW-SAF system.

by $r_{i,n}^{(2)} \in \Re^{4\times 1} = [r_{i,n}^{(2)}, r_{i+1,n}^{(2)}, r_{i+2,n}^{(2)}, r_{i+3,n}^{(2)}]^T$. The mathematical formulae to evaluate the parameters ρ and i at time index n for NSAF-2 are as follows:

$$i_n^{(2)} = \lfloor q[n]/\Delta u^{(2)} \rfloor + (R^{(2)} - 1)/2;$$

$$\rho_n^{(2)} = q[n]/\Delta u^{(2)} - \lfloor q[n]/\Delta u^{(2)} \rfloor \quad (4)$$

The response, $y[n]$ of the NSAF-2 block for the input, $q[n]$ is mathematically expressed as

$$y[n] = \rho_n^{(2)T} C r_{i,n}^{(2)} \quad (5)$$

where $\rho_{i,n}^{(2)} \in \Re^{4\times 1} = [\rho_{i,n}^{3(2)}, \rho_{i,n}^{2(2)}, \rho_{i,n}^{(2)}, 1]^T$ and the 4×4 spline basis matrix C is given in Eq. (3). Assuming that the signal $s[n]$ is the output of an unknown system corrupted with the additive Gaussian noise (zero mean and constant variance σ^2), the error signal $e[n]$ (Fig. 1) is given by $e[n] = s[n] - y[n]$, where $y[n]$ is given in Eq. (5).

Step 4: Fitness function formulation for the HW-SAF system design

In this study, the cost or fitness function (J_1) of the HW-SAF system is obtained as follows:

$$J_1(h_n, \rho_{i,n}^{(1)}, \rho_{i,n}^{(2)}) = (1/L) \times \sum_{l=1}^{L} e^2[l] \quad (6)$$

where L is the length of data samples.

A pictorial representation of the mathematical analysis of the above steps is presented in Fig. S1 (see supplementary material, Section 1) for better understanding.

2.2. Mathematical modelling of WH-SAF and its cost function formulation

A schematic diagram of a WH-SAF is shown in Fig. 2, where an NSAF is sandwiched between two linear filter (FIR) blocks (LF-1 and LF-2) (Scarpiniti et al., 2015b). Both LF-1 and LF-2 are designed with the FIR filter. The symbols corresponding to the LF-1 and LF-2 blocks are separately denoted by the superscripts 1 and 2. From Fig. 2, the output of the LF-1, NSAF and LF-2 blocks are mathematically expressed as follows (Scarpiniti et al., 2015b):

$$g[n] = h_n^{(1)T} u_n = \sum_{j=0}^{N_1} h_n^{(1)}[j] u[n-j] \quad (7)$$

$$q[n] = f(g[n], r_{i,n}) = \rho_n^T C r_{i,n} \quad (8)$$

$$y[n] = h_n^{(2)T} q_n = \sum_{k=0}^{N_2} h_n^{(2)}[k] q[n-k] \quad (9)$$

where $h_n^{(1)} \in \Re^{N_1\times 1} = [h_n^{(1)}[0], h_n^{(1)}[1], ..., h_n^{(1)}[n-N_1]]^T$ and $h_n^{(2)} \in \Re^{N_2\times 1} = [h_n^{(2)}[0], h_n^{(2)}[1], ..., h_n^{(2)}[n-N_2]]^T$ are the coefficient vectors of LF-1 and LF-2, respectively;

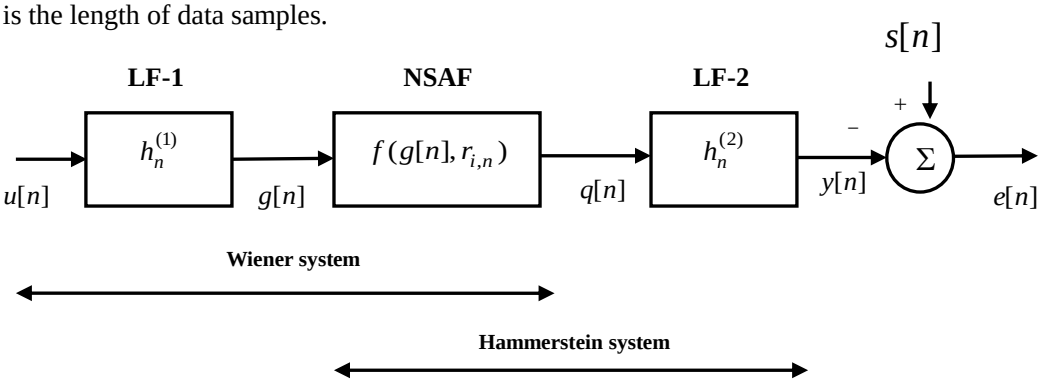

.

Fig. 2. Schematic diagram of a WH-SAF system.

Unedited

$u_n \in \Re^{N_1 \times 1} = [u[n], u[n-1],..., u[n-N_1+1]]^T$ is the input signal vector; the parameter $q_n \in \Re^{N_2 \times 1} = [q[n], q[n-1],..., q[n-N_2+1]]^T$; the local spline parameter $\rho_{i,n} \in \Re^{4\times 1} = [\rho_{i,n}^3, \rho_{i,n}^2, \rho_{i,n}, 1]^T$; the spline control points vector $r_{i,n} \in \Re^{4\times 1} = [r_{i,n}, r_{i+1,n}, r_{i+2,n}, r_{i+3,n}]^T$ and the 4×4 spline basis matrix C of size 4×4 are given in Eq. (3). The symbols N_1 and N_2 denote the lengths of the filter coefficients of LF-1 and LF-2, respectively. The error signal $e[n]$ (Fig. 2) is given by $e[n] = s[n] - y[n]$, where $y[n]$ is given in Eq. (9). The cost function (J_2) for the WH-SAF system is defined in Eq. (10).

$$J_2(h_n^{(1)}, h_n^{(2)}, r_{i,n}) = (1/L) \times \sum_{l=1}^{L} e^2[l] \tag{10}$$

In this study, the main aim of using MOA (i.e., ROA) was to minimise the cost function (J_1 or J_2) by jointly adapting the linear filter and spline control point weights. If J_1 or J_2 tends to zero, then the response of CSAF closely meets the actual output.

3 Proposed ROA-based CSAF design for unknown system modelling

MOAs are efficient in solving very complex problems (Janjanam et al., 2022b; Janjanam et al., 2023; Yan et al., 2023). Hence, in this study, various well-established MOAs such as ROA (Jia et al., 2021), MVO (Mirjalili et al., 2016), BSO (Shi et al., 2011) and DE (Storn et al., 1997) were individually applied to solve the parameter estimation problem of recently introduced CSAFs. Due to page constraints, we do not explain the basics and functional steps of MVO, BSO, and DE algorithms. Interested researchers may refer to Mirjalili et al. (2016), Shi et al. (2011), and Storn et al. (1997) for these algorithms. However, we present the step-by-step procedure of the ROA method for the design of CSAFs.

ROA (Jia et al., 2021) is a recently matured bio-inspired MOA that works on the principle of the parasitic behaviour and the random host replacement strategy of remora fish. The basic elementary details of the ROA can be found in (Jia et al., 2021). In ROA, the remora commonly follows the optimisation strategies of both humpback whales and swordfish. Hence, the ROA has the benefits of both the whale optimisation algorithm (WOA) (Mirjalili and Lewis 2016) and sailfish optimisation algorithm (SFO) (Shadravan et al., 2019) when dealing with optimisation problems.

To obtain optimal solutions, the ROA adopts the exploration (global search) and exploitation (local search) process by using the "free travel" and "eat thoughtfully" techniques, respectively. To perform the free travel operation, the ROA uses the methods of SFO and experiment attack. The WOA strategy and host feeding strategies are used to conduct eating techniques thoughtfully. The mathematical analysis to describe the position updating rules for this strategy was established by Jia et al. (2021) and was used in this study for the optimisation of cost functions, as given in Eqs (6) and (10).

The mechanism to design a CSAF for an unknown plant estimation using ROA proceeds mainly by initialization of search agents, fitness function evaluation for each search agent, and exploitation and exploration phases, which are discussed in detail below. The respective flowchart and pseudocode are shown in Fig. 3 and Table S1 (see supplementary material, Section 2), respectively.

Step 1: *Initialise the problem design variables (WH-SAF or HW-SAF parameters) in the search space*

Randomly develop NP number of search agents, where the position of each search agent is designated with the variables of the problem. The search space of each agent is filled with the parameters required to be optimised, such as spline control points (r_n) and linear filter coefficients (h_n). Moreover, randomly designate each parameter using

$$B_k^j = lb + rand \times (ub - lb),\ k \in 1,2,..., NP;\ j = 1,2,...\varpi \tag{11}$$

where *rand* produces the random values between 0 and 1, and the lower and upper boundaries of each parameter are represented by lb and ub , respectively. The vector representations of each agent (remora) for the HW-SAF and WH-SAF problems are given in Eqs (12) and (13), respectively. Moreover, the dimension

Unedited

of each agent is $(1\times\varpi)$, where ϖ denotes the total number of parameters. Therefore, the total dimension of NP number of agents is $(NP\times\varpi)$.

$$B^j = [h[0], h[1],..., h(N-1), r_1^{(1)}, r_2^{(1)},..., r_R^{(1)}, r_1^{(2)}, r_2^{(2)},..., r_R^{(2)}] \quad (12)$$

$$B^j = [h^{(1)}[0], h^{(1)}[1],..., h^{(1)}[n-N_1], h^{(2)}[0], h^{(2)}[1],..., h^{(2)}[n-N_2], r_1, r_2,..., r_R] \quad (13)$$

Step 2: *Evaluate the fitness of each remora*

Determine the fitness values for all the agents' positions using the fitness function (J_1 or J_2) as given in Eqs (6) and (10), then store the lowest error fitness value corresponding position (best) in (B_{best}).

Step 3: Determine the values of algorithm-specific parameters in each iteration

Amend the parameters β, γ and ξ using the following equations:

$$\beta = rand(0,1)\times(\gamma-1)+1 \quad (14)$$

$$\gamma = -(1+(t/T)) \quad (15)$$

$$\xi = 2(1-t/T) \quad (16)$$

where $rand(0,1)$ generates random numbers in [0, 1]; t is the current epoch number; T is the maximum epoch number; β takes random values in [-1, 1] and γ goes down linearly in [-2, -1].

Step 4: Perform exploitation and exploration mechanisms for each search agent

Repeat *Step i* to *Step iv* for each search agent, $k = 1,2,..., NP$.

(i) If the selection parameter $H(k) = 0$, then perform the eat method thoughtfully to achieve good exploitation (Jia et al., 2021). In this method, the position of the attached whales is updated using Eq. (17); otherwise, execute *Step 6*.

$$B_k(t+1) = D\times e^{\beta}\times\cos(2\pi\beta)+B_k(t) \quad (17)$$

where $B_k(t)$ is the current position; β is random values in [-1, 1] as given in Eq. (14), and D is the distance between the best and current positions, $D = \left|B_{best}(t)-B_k(t)\right|$.

(ii) If $H(k) = 1$, then carry out the free travel method for exploration, where the position of the attached sailfishes is updated using Eq. (18).

$$B_k(t+1) = B_{best}(t) - \Big(rand(0,1)\times... \left(\frac{B_{best}(t)+B_{rand}(t)}{2}\right) - B_{rand}(t)\Big) \quad (18)$$

where $B_{rand}(t)$ is the random position.

(iii) Construct a one-step prediction through experience attack. In this activity, the remora makes continuous small steps around the host to decide whether it is required to replace the host. This mechanism is given in Eq. (19) and formulated in (Jia et al., 2021).

$$B_{att}(t+1) = B_k(t) + randn\times(B_k(t)-B_{pre}(t)) \quad (19)$$

where $randn$ denotes the random small global Step; $B_{pre}(t)$ and $B_{att}(t)$ represent the previous generation's location and the location of the tentative Step, respectively.

(iv) If the fitness value of the attempted response $fit(B_{att}(t))$ is greater than the fitness value of the current response, $fit(B_k(t))$ then amend the position of the remora $B_k(t)$ with $B_{att}(t)$ and set $H(k)$ = round ($rand$). Conversely, if $fit(B_{att}(t)) < fit(B_k(t))$ then the remora chooses the host feeding phase for local optimisation. In this phase, the position of the remora is updated by the following (Jia et al., 2021):

$$B_k(t+1) = B_k(t+1) + F \quad (20)$$

$F = G\times(B_k(t)-V\times B_{best}(t))$, where

$$G = 2\times\xi\times rand(0,1)-\xi \quad (21)$$

where F denotes the small step change of the remora position, which corresponds to the volume space of the remora and host. To show the deviation between the position of the remora and the host, the remora factor V is used to narrow down the location of the remora. Also, the parameter ξ is defined in Eq. (16).

Step 5: *Confinement process*

Update the boundaries (lb and ub) if any agent escapes from the problem search space boundary. Also, update the position B_{best}.

Step 6: *Termination criterion for SMO algorithm*

Repeat *Step 2* to *Step 5* until the stopping condition (T) is reached and then declare B_{best} carries global optimised HW-SAF or WH-SAF system parameters.

Unedited

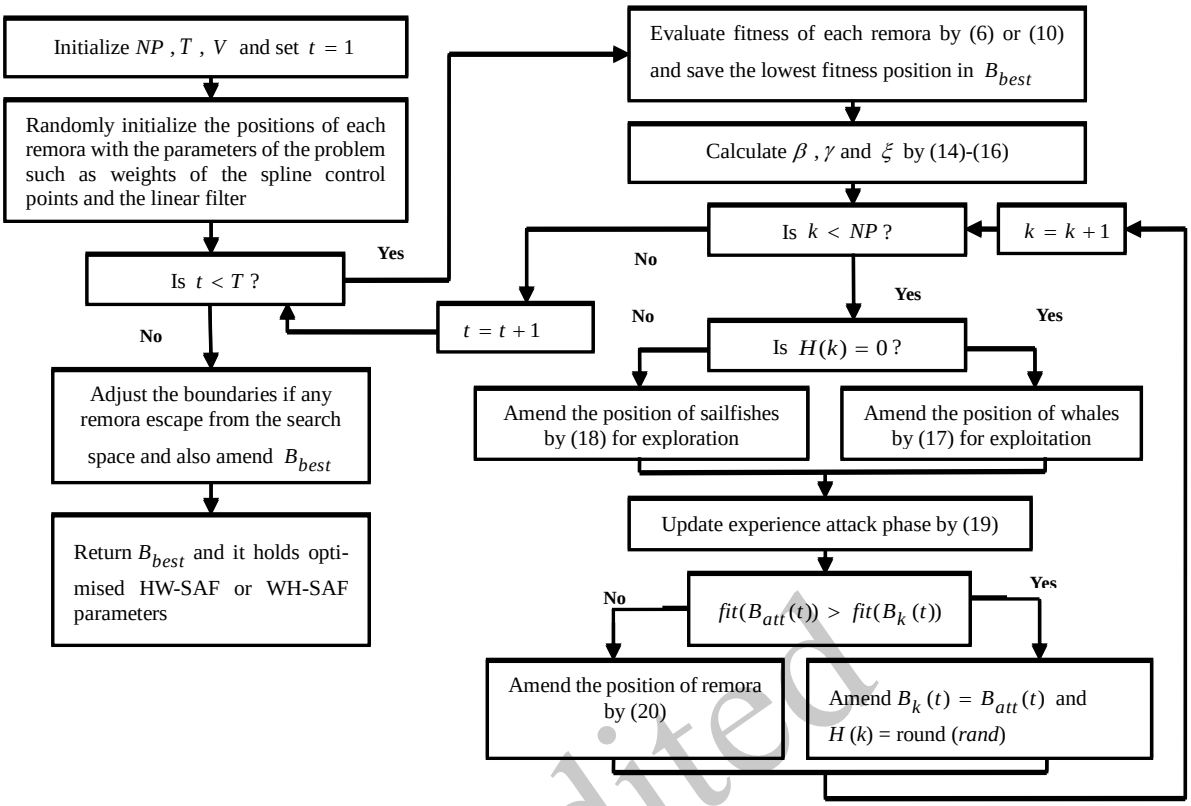

Fig. 3 Flow chart of CSAF system identification using the ROA method.

Unedited

4 Experimental Results and Analysis

In this section we present MATLAB software-based simulation results to demonstrate the effectiveness of the proposed ROA-based design technique for three numerical and two real-time systems. The first and second numerical systems have the HW-SAF and WH-SAF architectures, respectively, while the third system has HW architecture. Moreover, we have applied the respective architecture types to design the first and second systems. However, the third numerical system was identified using numerous well-known models. To substantiate the efficacy of the ROA-based design approach, three MOAs, namely MVO, BSO, and DE techniques, were independently applied to the same problem, and the various performance metrics obtained are compared.

The numerical values of the MOAs' control parameters vary based on the problem. Hence, we simulated each algorithm multiple times and chose the best set of control parameter values. We used the strategy described by Janjanam et al. (2022a) and Nayak et al. (2019) to fix the values of the lower bound (*lb*) and upper bound (*ub*) of the problem design variables, the number of populations (*NP*) and the maximum number of iterations (*T*). The selected *lb*, *ub*, *NP* and *T* values were -10,10, 25 and 1000, respectively. The justification for choosing these common control parameter values for all algorithms is provided in the supplementary material (Section 3). The other algorithm-specific parameter values, selected after performing exhaustive experiments and based on knowledge from the literature (Jia et al., 2021; Mirjalili et al., 2016; Shi et al., 2011; Storn et al., 1997) were as follows: (i) DE: cross over rate = 0.8 and scaling factor = 0.4; (ii) BSO: slope of logarithmic sigmoid function = 25, predefined probabilities $p_1 = 0.3$, $p_2 = 0.7$, $p_3 = 0.5$ and $p_4 = 0.4$; (iii) MVO: contrast parameter = 0.5, mining capability = 1/6, random parameters = [0, 1], wormhole existence probability = [0.3, 1] and travelling distance rate = [0, 1]; (iv) ROA: remora factor (V) = 0.5.

For a fair comparison, all algorithms were simulated on the same platform (64-bit Windows 7, Intel

i5 CPU, 3.20 GHz processor and 4 GB RAM). Moreover, 1100 random input data samples ($\in$[-1, 1]) were generated. The first 1000 samples were allotted for the identification (estimation) process, and the remaining 100 for the validation (testing) process.

4.1. Identification of unknown Systems 1 and 2

The mathematical forms of unknown nonlinear systems 1 and 2 are presented below and were identified in the same form as the estimation model.

System 1: System 1 (Scarpiniti et al., 2015b) is of WH-SAF architecture (Fig. 2). The coefficients of LF-1 and LF-2 blocks are presented mathematically in Eqs (22) and (23), respectively. In comparison, the nonlinear function of the NSAF block was modelled with the 23-point LUT having the control point vector r_n defined in Eq. (24) and Δu =0.2 (Scarpiniti et al., 2015b):

$$\text{LF-1: } h_n^{(1)} = [0.6, -0.4, 0.25, 0.1, -0.05, 0.001]^T \quad (22)$$

$$\text{LF-2: } h_n^{(2)} = [1, 0.5, -0.25, 0.15, 0.25, -0.10, 0.05]^T \quad (23)$$

$$\text{NSAF: } r_n = [-2.2, -2.0, -1.8, ..., -1.0, -0.8, -0.91, -0.40, -0.20, ... 0.05, 0.0, -0.40, 0.58, 1.0, 1.0, 1.2, 1.4, ..., 2.2]^T \quad (24)$$

System 2: System 2 (Scarpiniti et al., 2015b) is of HW-SAF architecture (Fig. 1). The internal blocks of HW-SAF structure, such as LF, NSAF-1 and NSAF-2, are mathematically described in Eqs (25)-(27), respectively, where the nonlinear functions of the two NSAF blocks are modelled with the 23 point LUT having the control points $r_n^{(1)}$ and $r_n^{(2)}$, respectively. Moreover, the spacing between the samples is Δu =0.2 (Scarpiniti et al., 2015b):

$$\text{LF: } h_n = [0.6, -0.4, 0.25, 0.1, -0.05, 0.001]^T \quad (25)$$

$$\text{NSAF-1: } r_n^{(1)} = [-2.2, -2.0, -1.8, ..., -1.0, -0.8, -0.91, -0.40, ... , -0.20, 0.05, 0.0, -0.40, 0.58, 1.0, 1.0, 1.2, 1.4, ..., 2.2]^T \quad (26)$$

$$\text{NSAF-2: } r_n^{(2)} = [-2.2, -2.0, -1.8, ..., -1.0, -0.8, -0.60, -0.10, ... -0.20, 0.0, 0.02, 0.40, 0.60, 0.8, 1.35, 1.2, 1.4, ..., 2.2]^T \quad (27)$$

4.1.1. Parameter convergence profiles

The best run convergence characteristics (out of 100 independent runs) for System 1 (WH-SAF) and System 2 (HW-SAF) using the proposed ROA-based design technique (at noise variance σ^2 = 0.001^2) are graphically illustrated in Fig. 4 and Fig. S2, respectively (supplementary material, Section 4 for Fig. S2). The spline control point vectors of each NSAF block of each system carry 23 coefficients (Eqs (24), (26) and (27)). However, due to space constraints, we present convergence profiles only for the most important coefficients of the control point vector (Figs 4, S2(b) and S2(c)), as recommended by Scarpiniti et al. (2013). Figs. 4 and S2 show that the linear filter (FIR) coefficients of both systems converged to their optimum values at about 580 iterations, and the NSAF control points took around 650 iterations. In addition, Fig. 4 shows that the achieved optimal values closely matched the true values. The various metrics (Mehmood et al., 2019a) such as MAE, RMSD, MWD and TIC results are presented in Table 1.

The absolute error (AE = $\left|\phi_m - \hat{\phi}_m\right|$) (Mehmood et al., 2019a) was used to measure the deviation between the achieved optimal estimated coefficients ($\hat{\phi}$) and the true coefficients($\hat{\phi}$). The values obtained for Systems 1-2 using the ROA, MVO, BSO and DE algorithms under three noise variance levels (σ^2 = 0.001^2, 0.01^2 and 0.1^2) are graphically presented in Fig. 5 and Fig. S3, respectively (see supplementary material, Section 5 for Fig. S3). The graphs are shown on a semi-logarithmic scale to increase visibility. Fig. 5 shows that the AE values of the System 1 design for the noise levels (σ^2) equal to 0.001^2, 0.01^2, and 0.1^2 lay in the range of 10^{-09} to 10^{-08} , 10^{-07} to 10^{-05}, and 10^{-05} to 10^{-04}, respectively, using the ROA; 10^{-08} to 10^{-07}, close to 10^{-06}, and 10^{-04}, respectively, using the MVO; 10^{-06} to 10^{-05}, 10^{-05} to 10^{-04}, and 10^{-04} , respectively, using the BSO; and finally 10^{-05} to 10^{-04}, 10^{-04} to 10^{-03}, and 10^{-02} to 10^{-01}, respectively, using the DE. From Fig. S3, the magnitudes of AE metric values of System 2 design for the noise variances (σ^2) equal to 0.001^2, 0.01^2, and 0.1^2 lay in the range of 10^{-07} to 10^{-06}, 10^{-05} to 10^{-04}, and 10^{-04} to 10^{-02}, respectively, using the ROA; 10^{-06} to 10^{-05}, 10^{-05} to 10^{-03}, and 10^{-03} to 10^{-02}, respectively, using the MVO; 10^{-05} to 10^{-04}, 10^{-03}, and 10^{-02}, respectively, using the BSO; and 10^{-03} to 10^{-02}, 10^{-02} to 10^{-01}, and 10^{-01} to 10^{0}, respectively, using the DE.

Unedited

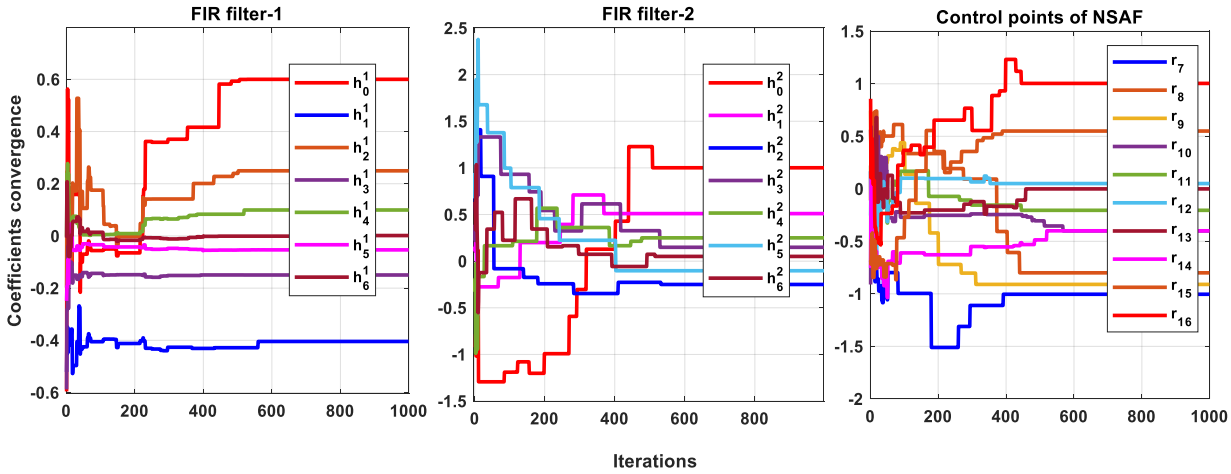

Fig. 4 Parameter convergence profiles of System 1 for the best run of the ROA technique.

From the above results, we have drawn the following conclusions: (i) the performance of each chosen MOA decreased with the rise in noise level, (ii) significantly lower values were achieved by using the ROA-based identification approach compared to others, and (iii) marginally superior AE results were achieved for System 1 (WH-SAF) than System 2 (HW-SAF) design using the MOAs because System 1 had less nonlinearity. Furthermore, the fitness function (Eqs (6) and (10)) was measured using the estimated coefficients obtained in the best simulation run. The fitness values secured in each iteration for Systems 1 and 2 modelling using the presented algorithms under different noise levels are shown in Fig. 6 and Fig. S4 (see supplementary material, Section 7), respectively, and the reported optimum fitness values are in Table 1 and Table S2. Table 1 and Table S2 also show the iteration number corresponding to the best fitness value and the computation time (CT) required by the chosen algorithm to complete 1000 iterations for the System 1 and 2 designs, respectively.

In the case of System 1 modelling, it is clear from Fig. 6 that for the three noise variance levels $\sigma^2 = 0.001^2$, 0.01^2, and 0.1^2, gave the optimum fitness order of 10^{-14}, 10^{-10}, and 10^{-09}, respectively, after completion of 509, 424, and 280 iterations by the ROA-based approach; 10^{-12}, 10^{-10}, and 10^{-08}, respectively, after 553, 435, and 289 iterations using the MVO; 10^{-09}, 10^{-08}, and 10^{-07}, respectively, after 569, 484, and 328 iterations using the BSO method; and 10^{-07}, 10^{-05}, and 10^{-03}, respectively, after 407, 385, and 257 iterations using the DE method.

Unedited

Table 1: Comparison of various performance indexes for the techniques used for the System 1 design

System	Method	Noise (σ^2)	Accuracy measures						
			MAE	RMSD	MWD	TIC	Fitness (J_1/J_2)	CT(s)	Iteration at best fitness
1	ROA	0.001^2	9.54E-09	1.76E-09	1.39E-08	3.21E-08	2.75E-14	0.432	509
		0.01^2	4.33E-08	8.92E-08	3.66E-07	4.56E-07	2.77E-10	0.424	424
		0.1^2	2.99E-06	3.11E-07	3.51E-06	1.76E-05	6.44E-09	0.437	280
	MVO	0.001^2	8.55E-08	6.54E-08	5.55E-07	3.65E-07	3.76E-12	0.625	553
		0.01^2	7.45E-06	7.43E-06	6.87E-06	4.87E-06	7.11E-10	0.620	435
		0.1^2	1.23E-05	5.98E-05	4.23E-04	1.67E-05	4.65E-08	0.617	289
	BSO	0.001^2	5.66E-07	4.76E-07	6.31E-05	3.89E-06	2.87E-09	0.901	569
		0.01^2	3.33E-06	4.54E-05	8.55E-04	2.54E-05	1.65E-08	0.893	484
		0.1^2	6.12E-04	6.36E-04	7.42E-03	1.43E-04	4.28E-07	0.899	328
	DE	0.001^2	1.98E-05	5.21E-04	3.37E-04	3.72E-03	3.65E-07	0.943	407
		0.01^2	3.22E-03	2.43E-03	8.22E-03	2.22E-02	2.83E-05	0.947	385
		0.1^2	2.43E-02	8.21E-03	3.54E-02	7.89E-02	3.47E-03	0.940	257

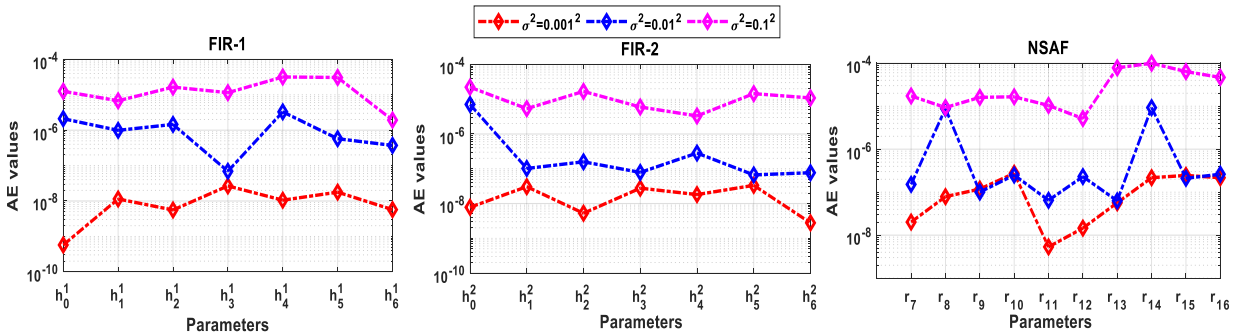

(a) ROA results for AEs

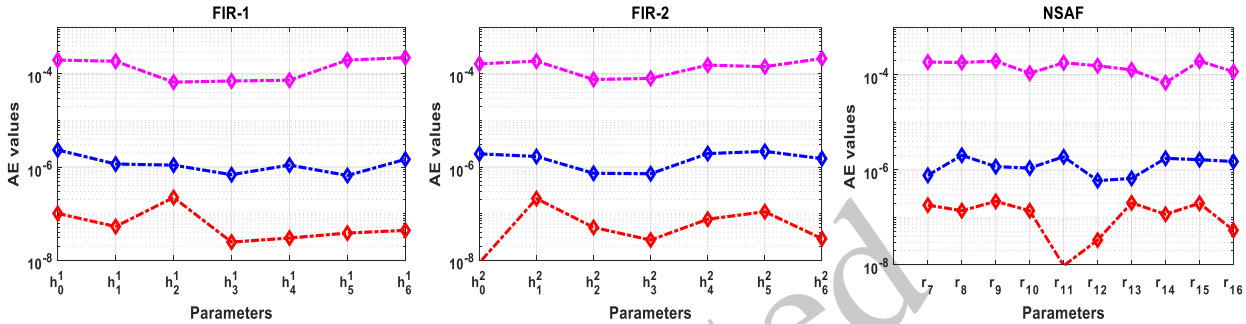

(b) MVO results for AEs

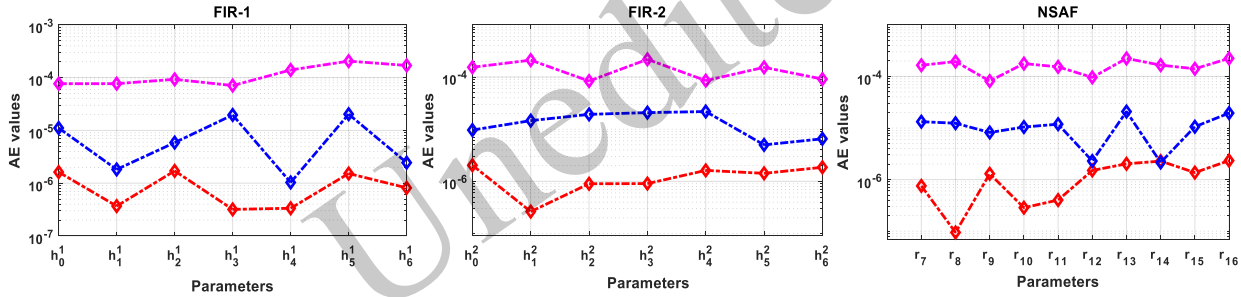

(c) BSO results for AEs

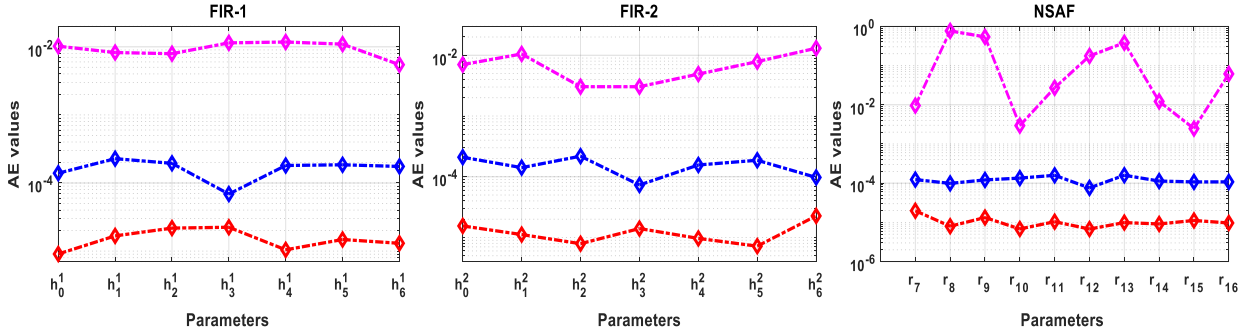

(d) DE results for AEs

Fig. 5 AE metric results for System 1 by the ROA, MVO, BSO, and DE algorithms under different noise levels.

Unedited

An analytical description of the fitness convergence profile for System 2 is provided in the supplementary material, Section 7. The convergence speed of the presented techniques was ordered: DE > ROA > MVO > BSO. The improvement (%) of the proposed ROA-based design technique over other chosen algorithms for the design of Systems 1 and 2 in terms of different metrics under the noise variance level $\sigma^2 = 0.001^2$ is shown in Fig. S5 (see supplementary material, Section 8). The improvement achieved using ROA over MVO, BSO and DE for

Systems 1 and 2 for the metrics lay in the range 88.84% to 99.99% and 76.89% to 99.99%, respectively.

4.1.2. Robustness performance analysis

In general, the performance of MOAs varies in each run (Jia et al., 2021). Hence, the robustness of the MOAs used for the design of Systems 1 and 2 was examined by simulating each algorithm in 100 independent runs. The statistics (best, worst and mean) of the estimated coefficients of Systems 1 and 2 obtained using the chosen algorithms under the noise level $\sigma^2 = 0.001^2$ are listed in Table 2 and Table S3, respectively (see supplementary material, Section 9 for Table S3).

Table 2: Statistical results of the estimated parameters of System 1 using chosen algorithms under the noisy condition $\sigma^2 = 0.001^2$

Method	Metric	FIR filter-1			FIR filter-2			NSAF			
		$h_0^{(1)}$	$h_3^{(1)}$	$h_6^{(1)}$	$h_0^{(2)}$	$h_3^{(2)}$	$h_6^{(1)}$	r_7	r_{10}	r_{13}	r_{16}
		0.6	-0.15	0.001	1.0	0.15	0.05	-1.0	-0.40	0.0	1.0
		$h_1^{(1)}$	$h_4^{(1)}$		$h_1^{(2)}$	$h_4^{(2)}$		r_8	r_{11}	r_{14}	
		-0.4	0.1	---	0.5	0.25	---	-0.8	-0.20	-0.40	---
		$h_2^{(1)}$	$h_5^{(1)}$		$h_2^{(2)}$	$h_5^{(2)}$		r_9	r_{12}	r_{15}	
		0.25	-0.05	---	-0.25	-0.10	---	-0.91	0.05	0.58	---
ROA	Best	0.600	-0.150	0.001	0.999	0.150	0.049	-1.000	-0.401	0.000	0.999
		-0.401	0.101	N/A	0.498	0.248	N/A	-0.798	-0.199	-0.402	N/A
		0.249	-0.050	N/A	-0.249	-0.101	N/A	-0.900	0.049	0.579	N/A
	Mean	0.601	-0.149	0.001	1.020	0.150	0.050	-1.001	-0.401	0.000	1.001
		-0.400	0.100	N/A	0.499	0.248	N/A	-0.799	-0.199	-0.402	N/A
		0.249	-0.049	N/A	-0.248	-0.100	N/A	-0.909	0.050	0.578	N/A
	Worst	0.598	-0.149	0.001	1.000	0.150	0.049	-0.098	-0.398	0.000	0.998
		-0.401	0.009	N/A	0.497	0.248	N/A	-0.798	-0.199	-0.401	N/A
		0.249	-0.049	N/A	-0.246	-0.095	N/A	-0.908	0.049	0.577	N/A
MVO	Best	0.589	-0.142	0.0009	0.961	0.141	0.042	-0.992	-0.396	0.001	0.989
		-0.388	0.093	N/A	0.445	0.239	N/A	-0.785	-0.192	-0.389	N/A
		0.240	-0.045	N/A	-0.234	-0.092	N/A	-0.892	0.048	0.571	N/A
	Mean	0.589	-0.143	0.0009	0.960	0.141	0.043	-0.993	-0.397	0.001	0.991
		-0.389	0.091	N/A	0.444	0.240	N/A	-0.786	-0.194	-0.390	N/A
		0.242	-0.044	N/A	-0.235	-0.091	N/A	-0.892	0.048	0.573	N/A
	Worst	0.588	-0.141	0.0009	0.959	0.140	0.040	-0.991	-0.395	0.001	0.988
		-0.387	0.090	N/A	0.443	0.240	N/A	-0.783	-0.194	-0.390	N/A
		0.240	-0.045	N/A	-0.235	-0.091	N/A	-0.890	0.048	0.570	N/A
BSO	Best	0.521	-0.132	0.0008	0.911	0.135	0.035	-0.936	-0.380	0.002	0.935
		-0.312	0.083	N/A	0.398	0.226	N/A	-0.716	-0.132	-0.329	N/A
		0.211	-0.038	N/A	-0.204	-0.083	N/A	-0.825	0.033	0.523	N/A
	Mean	0.520	-0.133	0.0008	0.910	0.134	0.035	-0.938	-0.381	0.002	0.936
		-0.313	0.085	N/A	0.399	0.227	N/A	-0.715	-0.135	-0.330	N/A
		0.213	-0.038	N/A	-0.205	-0.084	N/A	-0.827	0.033	0.525	N/A
	Worst	0.519	-0.133	0.0008	0.909	0.134	0.034	-0.934	-0.380	0.002	0.933
		-0.311	0.084	N/A	0.397	0.225	N/A	-0.712	-0.136	-0.330	N/A
		0.212	-0.039	N/A	-0.203	-0.082	N/A	-0.824	0.035	0.525	N/A
DE	Best	0.476	-0.124	0.0007	0.867	0.125	0.026	-0.889	-0.301	0.003	0.887
		-0.289	0.068	N/A	0.340	0.201	N/A	-0.701	-0.121	-0.301	N/A
		0.195	-0.033	N/A	-0.190	-0.072	N/A	-0.789	0.028	0.496	N/A
	Mean	0.477	-0.124	0.0007	0.866	0.124	0.025	-0.890	-0.302	0.003	0.889
		-0.290	0.069	N/A	0.342	0.202	N/A	-0.700	-0.123	-0.300	N/A
		0.194	-0.034	N/A	-0.192	-0.075	N/A	-0.788	0.029	0.498	N/A
	Worst	0.439	-0.126	0.0005	0.855	0.116	0.019	-0.857	-0.289	0.003	0.837
		-0.285	0.062	N/A	0.333	0.190	N/A	-0.695	-0.111	-0.289	N/A
		0.190	-0.031	N/A	-0.185	-0.067	N/A	-0.739	0.022	0.466	N/A

Unedited

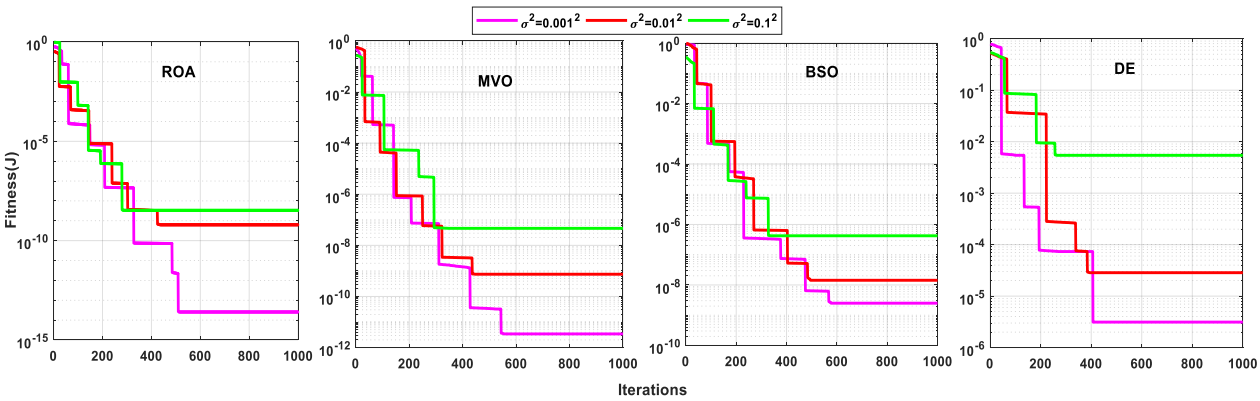

Fig. 6 Fitness convergence profiles for the System 1 design using the ROA, MVO, BSO, and DE algorithms under different noise levels.

Tables 2 and S3 show that the statistical results achieved through the ROA method were closer to the actual coefficients than those of other schemes. Moreover, there was no noticeable deviation between the results of the ROA and MVO techniques. However, both techniques outperformed the BSO and DE methods. Tables 2 and S3 also show that the mean results (average of 100 runs) of the ROA and DE schemes almost equal the best run result. Furthermore, the robustness of the MOAs used is also demonstrated through the global metrics such as GMAE, GRMSD, GTIC and GFIT (Mehmood.et al. 2019b). Each metric was measured using the estimation results of 100 independent simulations.The attained mean and standard deviation (STD) values corresponding to each metric for Systems 1 and 2 under different noise scenarios ($\sigma^2 = 0.001^2$, 0.01^2, and 0.1^2) are given in Table 3 and Table S4, respectively (refer to supplementary material, Section 10 for Table S4).

For System 1 and 2 designs, Tables 3 and S4 show that the mean values of the GFIT metric were around 10^{-14} to 10^{-07} for ROA, 10^{-13} to 10^{-08} for MVO, 10^{-09} to 10^{-05} for BSO, and 10^{-07} to 10^{-03} for DE. The range of magnitude levels for other global metrics, namely GMAE, GRMSD and GTIC, was from about 10^{-09} to 10^{-04} for ROA, 10^{-08} to 10^{-03} for MVO, 10^{-06} to 10^{-03} for BSO, and 10^{-05} to 10^{-01} for DE. Moreover, Tables 3 and S4 show that the mean values of all the global metrics correspond to the ROA, and DE algorithms are nearer to the best-run results (Table 1). Furthermore, the STD values of all the metrics corresponding to the ROA method (with the noise level $\sigma^2 = 0.001^2$) were closer to zero (from 10^{-14} to 10^{-09}) than those of the competing approaches.

Further, the fitness metric results on 100 independent runs of the ROA, MVO, BSO and DE algorithms for System 1 and 2 designs under various noise scenarios are graphically presented in Fig. 7 and Fig. S6, respectively (refer to supplementary material, Section 11 for Fig. S6). Figs. 7 and S6 show that the MVO and BSO algorithms showed substantial fluctuations. At the same time, DE and the proposed ROA-based design methods exhibited little volatility. However, the DE gave poor results. Thus, the independent test indicates that the proposed ROA-based approach shows more robust performance and is statistically significantly better than others. Additionally, the consistency of performance of the ROA over the MVO, BSO and DE algorithms for the design of CSAFs (Systems 1 and 2) was verified using Holm's test (Shadravan et al., 2019; Holm 1979; Braik et al., 2022). The procedure for conducting Holm's test and results obtained for both systems are provided in supplementary material Section 12.

4.1.3. Computational complexity analysis

Generally, a particular technique's computational complexity (CC) is denoted by '*O*-notation'. The CC of the algorithms used for the chosen System 1 (HW-SAF) and System 2 (WH-SAF) were calculated based on the literature (Janjanam et al., 2022d; Jia et al., 2021; Yadav et al., 2023). The CC of the MOA used is $O(MOA) = O(F(x)) \times O\left(NP \times \left(T\varpi + 1\right)\right)$ (refer to supplementary material, Section 13 for the proof), where $F(x)$ denotes the fitness function of the chosen problem, NP is the population size, T is the maximum iteration number and ϖ is the dimension of the problem.

Unedited

Table 3: Statistical analysis of the global metric results for System 1 using chosen algorithms under different noisy conditions

Sys	Method	Noise (σ^2)	Global measures							
			GMAE		GRMSD		GTIC		GFIT	
			Mean	STD	Mean	STD	Mean	STD	Mean	STD
1	ROA	0.001^2	8.54E-09	2.21E-09	2.55E-09	2.55E-10	7.69E-08	5.32E-11	4.09E-14	1.33E-14
		0.01^2	5.98E-08	4.33E-07	7.21E-08	4.37E-08	2.13E-07	4.47E-09	5.54E-10	5.92E-13
		0.1^2	6.65E-06	5.47E-06	3.79E-07	3.66E-07	4.25E-05	6.23E-07	7.61E-09	4.71E-11
	MVO	0.001^2	3.22E-07	4.56E-08	3.76E-08	2.55E-07	5.78E-08	5.98E-10	7.50E-13	1.06E-12
		0.01^2	3.12E-06	4.89E-06	1.98E-06	4.69E-06	3.69E-06	4.47E-08	8.35E-11	5.57E-10
		0.1^2	6.79E-04	3.97E-05	2.70E-05	2.96E-04	2.87E-05	3.78E-07	9.51E-09	1.95E-09
	BSO	0.001^2	1.87E-05	3.76E-09	7.32E-06	3.87E-08	7.58E-06	5.67E-12	7.53E-09	2.28E-10
		0.01^2	5.38E-04	6.43E-05	4.38E-05	5.93E-05	6.75E-05	2.59E-08	1.39E-07	9.38E-07
		0.1^2	5.77E-03	4.57E-04	1.89E-03	3.58E-04	5.91E-04	3.85E-06	5.24E-05	6.33E-06
	DE	0.001^2	7.93E-05	7.85E-04	2.78E-04	4.66E-06	2.66E-03	4.69E-04	2.57E-07	4.57E-08
		0.01^2	5.33E-03	5.37E-03	3.97E-03	9.88E-03	4.58E-02	7.56E-03	5.06E-05	5.24E-06
		0.1^2	6.68E-02	3.78E-03	7.74E-03	5.23E-02	8.29E-02	4.42E-02	3.95E-03	7.09E-03

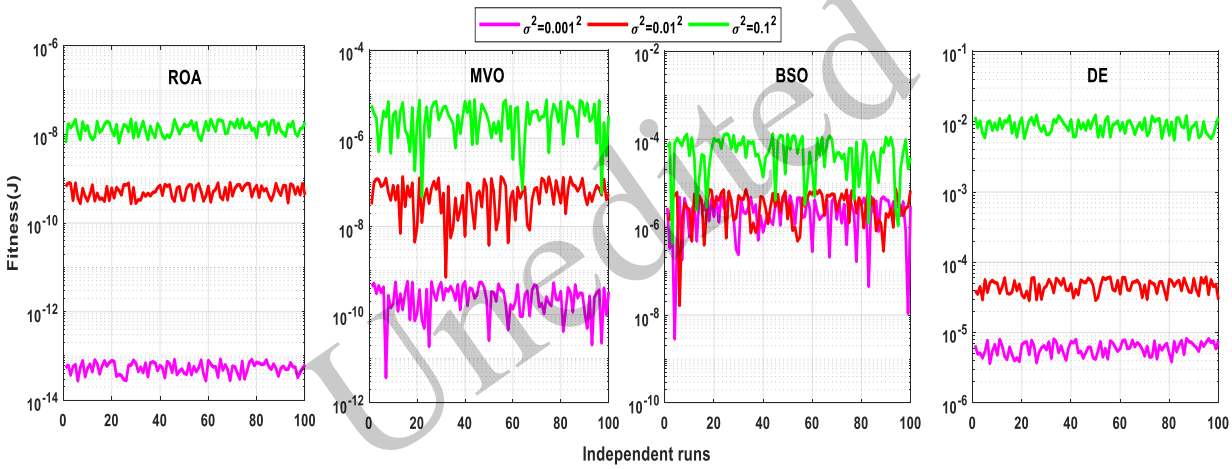

Unedited

Fig. 7 Independent run results of the fitness metric for System 1 using the considered algorithms at various noise

In this study, the CC of the algorithms used for modelling Systems 1 and 2 was also examined with the help of runtime. Consider the computational time (CT), CT for one iteration, $T_0(=CT/T\times NP)$, $T_1(=CT/T)$ and T_2 (= Average time of 'K' independent runs), respectively (Janjanam et al., 2022d; Yadav et al., 2023). The calculated values for T_0, T_1 and T_2 metrics (at K=100, NP=25 and T=1000) for modelling each system are listed in Table 4. Table 4 shows that the proposed ROA-based design scheme takes less run time than other MVO-, BSO-, and DE-based design schemes.

4.2. System 3: Nonlinear HW system identification using well-known models

The nonlinear block outputs ($g[n]$ and $y[n]$) of the HW system and its FIR filter transfer function ($H(z)$) are given as follows (Scarpiniti.et al. 2015b):

$$g[n]=u[n]\Big/\sqrt{0.1+0.9u^2[n]},\ y[n]=q[n]-0.5q^2[n]+0.2q^3[n],$$
$$H(z)=1-0.25z^{-1}+0.05z^{-2}+0.001z^{-3} \quad (28)$$

In this study, the above HW system was identified using the ROA along with different popular models such as the third order Volterra model (Schetzen 1981), Jeraj and Mathews model (Jeraj 2006), Hegde et al. (2002a and 2002b) LNL model, WSAF (Scarpiniti et al., 2013), HSAF (Scarpiniti et al., 2014), WH-SAF and HW-SAF. Moreover, 1150 random input samples ($\in$ [-1 1]) were generated for the System 3 design, in which a total of 1000 and 150 samples were separately allotted for the estimation and validation, respectively, of the model.

Table 4: CC and run time results of Systems 1 and 2 designs using the chosen algorithms

System	Metric	Algorithms			
		ROA	MVO	BSO	DE
1	T_0 (s)	1.732E-05	2.500E-05	3.604E-05	3.772E-05
	T_1 (s)	4.32E-04	6.25E-04	9.07E-04	9.43E-04
	T_2 (s)	0.426	0.618	0.893	0.940
	CC	$O(F(x))\times O\left(NP\times\left(T\varpi+1\right)\right)$	$O(F(x))\times O\left(NP\times\left(T\varpi+1\right)\right)$	$O(F(x))\times O\left(NP\times\left(T\varpi+1\right)\right)$	$O(F(x))\times O\left(NP\times\left(T\varpi+1\right)\right)$
2	T_0 (s)	2.244E-05	2.932E-05	3.948E-05	4.452E-05
	T_1 (s)	5.61E-04	7.33E-04	9.87E-04	1.113E-03
	T_2 (s)	0.554	0.728	0.983	1.108
	CC	$O(F(x))\times O\left(NP\times\left(T\varpi+1\right)\right)$	$O(F(x))\times O\left(NP\times\left(T\varpi+1\right)\right)$	$O(F(x))\times O\left(NP\times\left(T\varpi+1\right)\right)$	$O(F(x))\times O\left(NP\times\left(T\varpi+1\right)\right)$

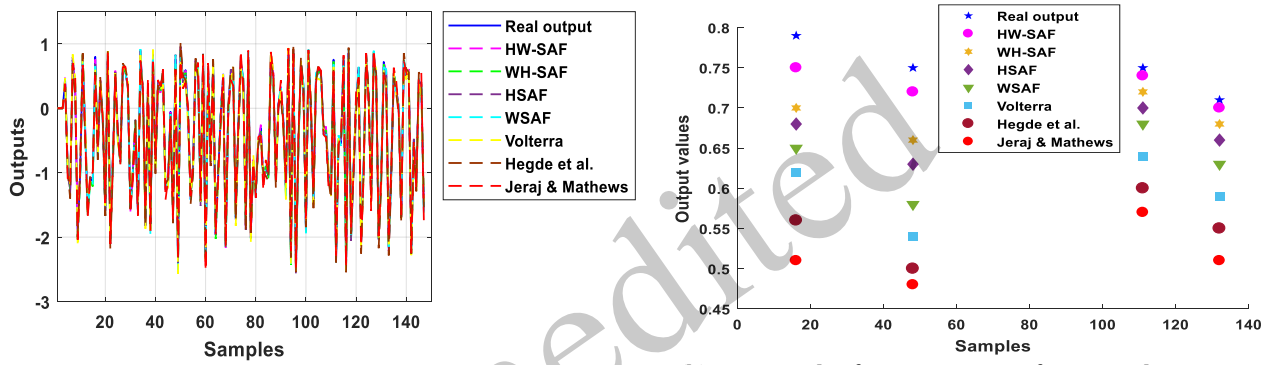

(a) Comparison of real and estimated outputs (b) Scatter plot for comparison of estimated output

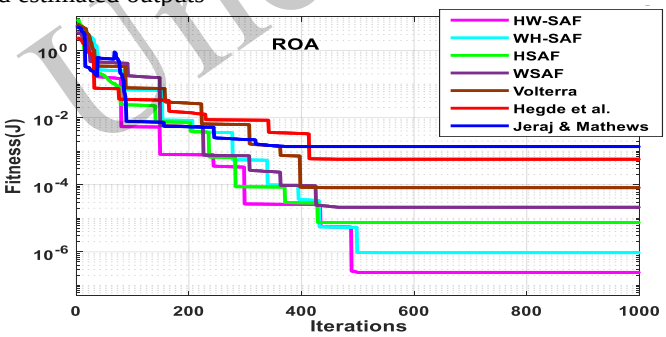

(c) Fitness convergence plot

Fig. 8 Identification results of System 3 using different models based on the ROA method.

Unedited

The actual and estimated outputs from the above models for the System 3 design from the validation data input are shown in Fig. 8(a). It is apparent that the estimated plots of all the models are close to the actual output. To show the deviation among them, a scatter plot was drawn using a few carefully chosen samples (Fig. 8(b)). Fig. 8(b) shows that the estimated output values of the HW-SAF and WH-SAF models are closer to the real ones. The fitness convergence plots for System 3 are shown in Fig. 8(c). The plots for System 3 are shown in Fig. 8(c). The approaches presented took 320 to 500 iterations to converge to their optimal solutions. The optimum fitness values obtained (after 1000 iterations) are given in Table 5. Moreover, the percentage of quality of fitness

$$QF(\%)=\left(1-\frac{1}{L}\sum_{n=1}^{L}(y[n]-\hat{y}[n])^2\Big/\frac{1}{L}\sum_{n=1}^{L}(y[n])^2\right)\times 100$$

was evaluated. The measured values for all approaches are reported in Table 5, and the measured QF (%) was 90.22% and 92.65% using WH-SAF and HW-SAF models, respectively

Table 5: Fitness and QF(%) metric values comparison of different identification models for the design of System 3

Method	Metric	Identification models						
		Jeraj and Mathews	Hegde *et al.*	Volterra	WSAF	HSAF	WH-SAF	HW-SAF
ROA	Fitness	1.33E-03	5.76E-04	8.16E-05	2.13E-05	7.45E-06	9.44E-07	2.35E-07
	QF (%)	72.33	74.78	79.24	81.33	87.59	90.22	92.65

4.3. Real-time systems identification

In this study, two real-time systems, namely, coupled electric drives and thermic wall benchmark systems, were identified using the ROA-based WH-SAF and HW-SAF models.

4.3.1. System 4: Coupled electric drive system identification

The basic details of coupled electric drives (Wigren et al. 2013) are provided in supplementary material Section 14. Out of 500 input and output (I/O) samples, 400 I/O were chosen for estimation and 100 I/O to validate the system (Fig. S7). We used the ROA, MVO, BSO and DE techniques to optimise the HW-SAF (with N = 5, B-spline and $\Delta u^{(1)} = \Delta u^{(2)} = 0.2$) and WH-SAF (with $N_1 = N_2 = 5$, B-spline and $\Delta u = 0.2$) structures for the estimation of System 4.

The secured optimum fitness and *QF* (%) metric values for the drive-1 and drive-2 datasets are listed in Table 6. Better results were achieved with the WH-SAF structure than with HA-SAF for all the techniques. Moreover, significantly improved results were achieved using ROA compared to MVO, BSO and DE algorithms. Also, a slightly improved result was observed using the drive-2 datasets compared to the drive-1 datasets. The best fitness values for the System 4 design using the ROA-, MOA-, BSO-, and DE-based WH-SAF approaches were 8.33E-06, 1.37E-05, 3.66E-03 and 4.92E-02, respectively. Meanwhile, the QF (%) results for the respective algorithms were 92.52%, 90.45%, 86.21%, and 83.61%.

Unedited

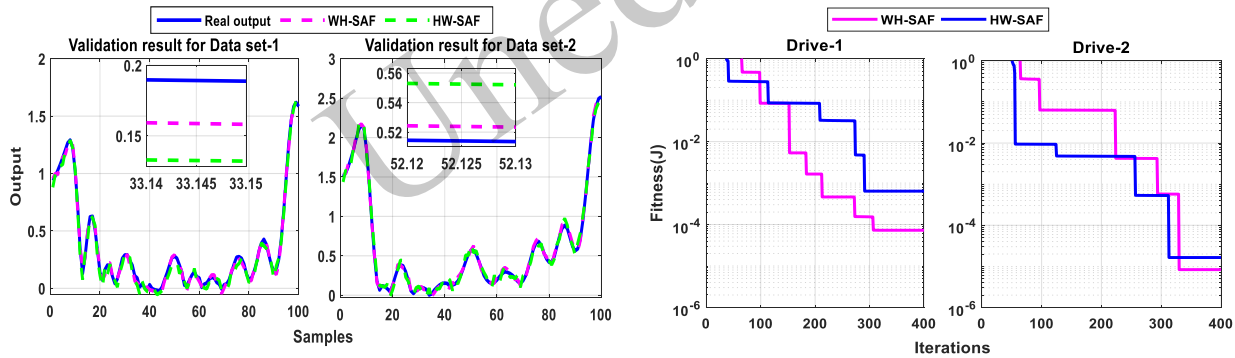

(a) Comparison of validation outputs (b) Fitness convergence plots for drive-1 and 2 data sets

Fig. 9 Identification results of System 4 (coupled electric drives system) using different models based on ROA.

Table 6: Comparison of fitness and QF (%) metric values of different identification models for the design of System 4 using ROA, MVO, BSO and DE techniques

Method	Metric	Drive-1		Drive-2	
		WH-SAF	HW-SAF	WH-SAF	HW-SAF
ROA	Fitness	7.28E-05	6.38E-04	8.33E-06	1.64E-05
	QF (%)	91.87	90.56	93.76	92.52
MVO	Fitness	2.62E-03	7.66E-03	1.37E-05	3.56E-04
	QF (%)	88.46	87.12	91.45	90.45
BSO	Fitness	3.33E-02	9.67E-02	3.66E-03	7.34E-03
	QF (%)	85.32	83.95	87.56	86.21
DE	Fitness	9.55E-02	3.57E-01	4.92E-02	2.78E-02
	QF (%)	82.67	80.75	84.47	83.61

Fig. 9(a) show the validation results using the proposed RSA-based design for the drive-1 and drive-2 datasets, respectively. The WH-SAF-based estimated output plot is nearer to the actual output than the HW-SAF-based plot. The convergence of fitness values for the drive-1 and drive-2 datasets for System 4 design using the proposed RSA-based design is shown in Fig. 9(b). Both models took around 290 to 340 iterations for convergence.

4.3.2. System 5: Thermic wall system identification

This study identified the thermic wall system by taking the input (external temperature) and output (heat flow density) datasets from the Daisy database (De Moor 2004). From a total of 1680 samples, sets of 1200 and 480 data samples, respectively, were used for estimation and validation purposes (Fig. 10(a)).

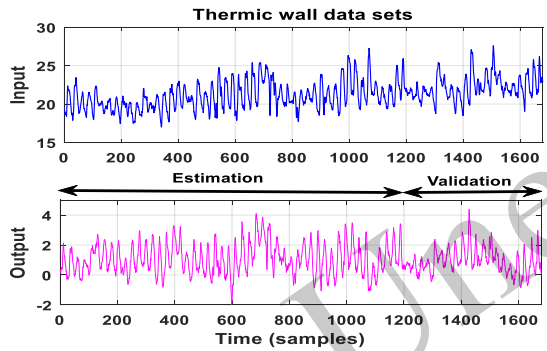

(a) I/O data sets (De Moor 2004)

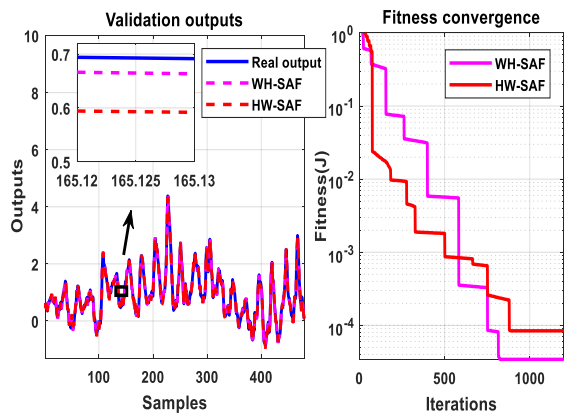

(b) Comparison of validation outputs and fitness convergence

Fig. 10 Identification results of System 5 (thermic wall system) using different models based on ROA.

The fitness and *QF* (%) metric results obtained for System 5 modelling using ROA, MVO, BSO, and DE techniques are shown in Table 7. The best fitness and *QF* (%) metric results achieved from the proposed ROA were 3.43E-05 and 92.65%, respectively. Meanwhile, the nearest competitor (MVO) produced a fitness of 2.75E-04 and *QF* (%) of 90.13%, respectively. Finally, the DE gave significantly lower quality results (fitness of 9.95 and QF of 80.42%) than others. The results achieved for validation outputs and convergence speed of the fitness function for the thermic wall system by the proposed ROA-based HW-SAF and WH-SAF models are shown in Fig. 10(b). From Fig. 10(b), the schemes presented exhibit good tracking accuracy compared with the actual output, and achieved the best fitness value with the WH-SAF and HW-SAF models after 810 and 892 iterations, respectively.

Table 7: Comparison of fitness and QF (%) metrics of different identification models for the design of System 5

Method	Metric	Identification models	
		WH-SAF	HW-SAF
ROA	Fitness	3.43E-05	8.41E-05
	QF (%)	92.65	91.72
MVO	Fitness	2.75E-04	6.67E-04
	QF (%)	90.13	89.16
BSO	Fitness	1.56E-02	7.83E-02
	QF (%)	86.45	85.33
DE	Fitness	4.67	9.95
	QF (%)	81.76	80.42

4.3.3. System 6: CSTR plant estimation

The details of the CSTR plant and its datasets are briefly discussed in the supplementary material, Section 15. To model the CSTR using the HW-SAF and WH-SAF models, the actual input coolant flow-rate $q_c(t)$ and output concentration $C_A(t)$ (Janjanam et al., 2022b; Lightbody and Irwin 1997; Hafezi and Arefi 2019) datasets were collected from the DAISY database (De Moor 2004). The achieved fitness and *QF* (%) metric results for System 6 using all the algorithms for both structures are presented in Table 8. The WH-SAF model showed superior performance compared to the HW-SAF model. The best fitness values achieved for ROA, MVO, BSO, and DE methods were 1.45E-04, 2.36E-03, 4.58E-01, and 6.49, respectively. In comparison, the *QF* metric results of the respective algorithms were 90.36%, 88.66%, 84.32% and 80.35%. The fitness conver-

Unedited

gence behaviour for the best algorithm (ROA) with WH-SAF and HW-SAF structures for the CSTR system modelling is depicted in Fig. 11(a) and converged after 616 and 771 iterations, respectively. We derived the estimated output using the optimised WH-SAF model and the validation data input samples, closely tracking the actual output (Fig. 11(b)).

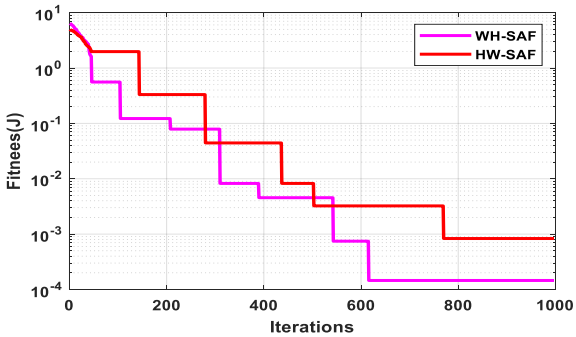

(a) Fitness convergence behaviour

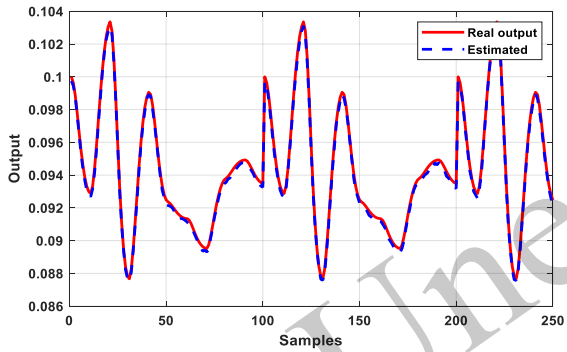

(b) Real and estimated outputs

Fig. 11. CSTR plant identification results using ROA

Table 8: Comparison of fitness and QF metric values of different identification models for the design of System 6

Method	Metric	Identification models	
		WH-SAF	HW-SAF
ROA	Fitness	1.45E-04	8.36E-04
	QF (%)	90.36	89.65
MVO	Fitness	2.36E-03	6.73E-03
	QF (%)	88.66	87.53
BSO	Fitness	4.58E-01	9.67E-02
	QF (%)	84.32	83.21
DE	Fitness	6.49	8.65
	QF (%)	80.35	79.33

5 Conclusions and future directions

In this is study, two recently proposed novel CSAFs, WH-SAF and HW-SAF, were effectively identified using the ROA technique. The ROA optimises spline control points and linear filter coefficients jointly using the formulated objective function, enhancing performance stability. The comparative study of other competent algorithms, such as MVO, BSO and DE, for the exact problem identification, revealed that the proposed ROA-based design scheme yields highly accurate estimated parameters with better convergence speed. The statistical results of numerous performance indices and the performance comparison of algorithms under various noise levels $\sigma^2 = 0.001^2$, 0.01^2 and 0.1^2 confirmed that the proposed design approach is more statistically significant, reliable, robust and stable than the others. The results of the statistical hypothesis test showed that the ROA- and DE-based design schemes had a more consistent performance than those of MVO- and BSO-based approaches. However, the DE scheme provides substantially lower quality results than the others. Moreover, various attractive models, as discussed by Scarpiniti et al. (2015b) were applied for designing a nonlinear HW system, which yielded significantly improved results using WH-SAF and HW-SAF models. Additionally, the estimation results of coupled electric drives, thermic wall systems and CSTR showed the real strength of the proposed ROA-based CSAF design approach in a practical scenario. For future scope, the proposed methods will be extended to multiple-input and multiple-output systems and will be used to solve the estimation problems of multi-dimensional real-time nonlinear plants.

Unedited

Contributors

Lakshminarayana JANJANAM: Conceptualization, Methodology, Software, Writing – original draft; Suman Kumar SAHA: Writing – review & editing, Data curation; Rajib KAR: Visualization, Investigation, Supervision

Conflict of interest

All the authors declare that they have no conflict of interest.

References

Braik M, Hammouri A, Atwan J, et al., 2022. White shark optimizer: a novel bio-inspired meta-heuristic algorithm for global optimization problems. *Knowl-Based Syst*, 243:108457. https://doi.org/10.1016/j.knosys.2022.108457

Chaudhary NI, Manzar MA, Raja MAZ, 2019. Fractional

volterra LMS algorithm with application to hammerstein control autoregressive model identification. *Neural Comput Appl*, 31(9):5227-5240. https://doi.org/10.1007/s00521-018-3362-z

Chen ZY, Meng YH, Chen T, 2022. NN model-based evolved control by DGM model for practical nonlinear systems. *Expert Syst Appl*, 193:115873. https://doi.org/10.1016/j.eswa.2021.115873

De Moor B, 2004. Database for identification of systems. *KU. Leuven: Department of Electrical Engineering*. http://homes.esat.kuleuven.be/~smc/~daisy/

Esmaeilani L, Ghaisari J, Bagherzadeh MA, 2021. Hammerstein–Wiener identification of industrial plants: a pressure control valve case study. *IET Control Theory Appl*, 15(3):416-431. https://doi.org/10.1049/cth2.12052

Gao Y, Zhao HQ, ZhuYY, et al., 2023. Spline adaptive filtering algorithm-based generalized maximum correntropy and its application to nonlinear active noise control. *Circuits Syst Signal Process*, 42(11):6636-6659. https://doi.org/10.1007/s00034-023-02411-5

Gao Y, Zhao HQ, Zhu YY, et al., 2024. The q-gradient LMS spline adaptive filtering algorithm and its variable step-size variant. *Inf Sci*, 658:119983. https://doi.org/10.1016/j.ins.2023.119983

Garcia-Vega S, Zeng XJ, Keane J, 2020. Stock returns prediction using kernel adaptive filtering within a stock market interdependence approach. *Expert Syst Appl*, 160:113668. https://doi.org/10.1016/j.eswa.2020.113668

Guan SH, Biswal B, 2023. Spline adaptive filtering algorithm based on different iterative gradients: performance analysis and comparison. *J Autom Intell*, 2(1):1-13. https://doi.org/10.1016/j.jai.2022.100008

Guan SH, Cheng Q, Zhao Y, et al., 2022. Spline adaptive filtering algorithm based on Heaviside step function. *Signal Image Video Process*, 16(5):1333-1343. https://doi.org/10.1007/s11760-021-02085-z

Guo WY, Zhi YF, 2022. Nonlinear spline adaptive filtering against non-Gaussian noise. *Circuits Syst Signal Process*, 41(1):579-596. https://doi.org/10.1007/s00034-021-01798-3

Guo WY, Zhi YF, Feng K, 2022. Nonlinear spline prioritization optimization adaptive filter with arctangent-exponential hyperbolic cosine. *Nonlinear Dyn*, 110(1):611-621. https://doi.org/10.1007/s11071-022-07636-8

Hafezi Z, Arefi MM, 2019. Recursive generalized extended least squares and RML algorithms for identification of bilinear systems with ARMA noise. *ISA Trans*, 88:50-61. https://doi.org/10.1016/j.isatra.2018.12.015.

Hammar K, Djamah T, Bettayeb M, 2019. Nonlinear system identification using fractional Hammerstein–Wiener models. *Nonlinear Dyn*, 98(3):2327-2338. https://doi.org/10.1007/s11071-019-05331-9

Hegde V, Radhakrishnan C, Krusienski DJ, et al., 2002a. Architectures and algorithms for nonlinear adaptive filters. Conf Record of the Thirty-Sixth Asilomar Conf on Signals, Systems and Computers, p.1015-1018. https://doi.org/10.1109/ACSSC.2002.1196937

Hegde V, Radhakrishnan C, Krusienski D, et al., 2002b. Series-cascade nonlinear adaptive filters. The 45th Midwest Symposium on Circuits and Systems, p.III-219-III-222. https://doi.org/10.1109/MWSCAS.2002.1187010

Holm S, 1979. A simple sequentially rejective multiple test procedure. *Scand J Stat*, 6(2):65-70.

Janjanam L, Saha SK, Kar R, et al., 2021a. An efficient identification approach for highly complex non-linear systems using the evolutionary computing method based Kalman filter. *AEU Int J Electron Commun*, 138:153890. https://doi.org/10.1016/j.aeue.2021.153890

Janjanam L, Saha SK, Kar R, et al., 2021b. Global gravitational search algorithm-aided Kalman filter design for volterra-based nonlinear system identification. *Circuits Syst Signal Process*, 40(5):2302-2334. https://doi.org/10.1007/s00034-020-01593-6

Janjanam L, Saha SK, Kar R, et al., 2022a. Hammerstein-Wiener nonlinear system identification by using honey badger algorithm hybridized Sage-Husa adaptive Kalman filter with real-time applications. *AEU Int J Electron Commun*, 151:154218. https://doi.org/10.1016/j.aeue.2022.154218

Janjanam L, Saha SK, Kar R, et al., 2022b. Improving the modelling efficiency of Hammerstein system using Kalman filter and its parameters optimised using social mimic algorithm: application to heating and cascade water tanks. *J Franklin Inst*, 359(3):1239-1273. https://doi.org/10.1016/j.jfranklin.2021.12.022

Janjanam L, Saha SK, Kar R, et al., 2022c. Optimal design of cascaded Wiener-Hammerstein system using a heuristically supervised discrete Kalman filter with application on benchmark problems. *Expert Syst Appl*, 200:117065. https://doi.org/10.1016/j.eswa.2022.117065

Janjanam L, Saha SK, Kar R, et al., 2022d. Wiener model-based system identification using moth flame optimised Kalman filter algorithm. *Signal Image Video Process*, 16(5):1425-1433. https://doi.org/10.1007/s11760-021-02096-w

Janjanam L, Saha SK, Kar R, 2023. Optimal design of hammerstein cubic spline filter for nonlinear system modeling based on snake optimiser. *IEEE Trans Ind Electron*, 70(8):8457-8467. https://doi.org/10.1109/TIE.2022.3213886

Jeraj J, Mathews VJ, 2006. A stable adaptive Hammerstein filter employing partial orthogonalization of the input

Unedited

signals. *IEEE Trans Signal Process*, 54(4):1412-1420. https://doi.org/10.1109/TSP.2006.870643

Jia HM, Lang CB, Oliva D, et al., 2019. Dynamic Harris hawks optimization with mutation mechanism for satellite image segmentation. *Remote Sens*, 11(12):1421. https://doi.org/10.3390/rs11121421

Jia HM, Peng XX, Lang CB, 2021. Remora optimization algorithm. *Expert Syst Appl*, 185:115665. https://doi.org/10.1016/j.eswa.2021.115665

Jia HM, Rao HH, Wen CS, et al., 2023. Crayfish optimization algorithm. *Artif Intell Rev*, 56(2):1919-1979. https://doi.org/10.1007/s10462-023-10567-4

Jia L, Feng Q L, 2017. Combined separable signals based neuro-fuzzy Hammerstein–Wiener model. *Memetic Comput*, 9(3):245-259. https://doi.org/10.1007/s12293-016-0204-3

Li LW, Ren XM, 2018. Identification of nonlinear Wiener-Hammerstein systems by a novel adaptive algorithm based on cost function framework. *ISA Trans*, 80:146-159. https://doi.org/10.1016/j.isatra.2018.07.015

Li WQ, Xu M, Tang JS, et al., 2023. Robust frequency domain spline adaptive filtering based on the half-quadratic criterion: performance analysis and applications. *IEEE Trans Instrum Meas*, 72:6503513. https://doi.org/10.1109/TIM.2023.3271721

Lightbody G, Irwin GW, 1997. Nonlinear control structures based on embedded neural system models. *IEEE Trans Neural Netw*, 8(3):553-567. https://doi.org/10.1109/72.572095

Liu C, Zhao HQ, 2023. A 2D-LUT scheme design for complex-valued spline adaptive filter. *IEEE Trans Circuits Syst II: Express Briefs*, 70(8):3154-3158. https://doi.org/10.1109/TCSII.2023.3245670

Liu Q, Tang XM, Li JH, et al., 2021. Identification of Wiener–Hammerstein models based on variational Bayesian approach in the presence of process noise. *J Franklin Inst*, 358(10):5623-5638. https://doi.org/10.1016/j.jfranklin.2021.05.003

Mehmood A, Raja MAZ, 2023. Novel design of weighted differential evolution for parameter estimation of Hammerstein-Wiener systems. *J Adv Res*, 43:123-136. https://doi.org/10.1016/j.jare.2022.02.010

Mehmood A, Zameer A, Chaudhary NI, et al., 2019a. Backtracking search heuristics for identification of electrical muscle stimulation models using Hammerstein structure. *Appl Soft Comput*, 84:105705. https://doi.org/10.1016/j.asoc.2019.105705

Mehmood A, Chaudhary NI, Zameer A, et al., 2019b. Backtracking search optimization heuristics for nonlinear Hammerstein controlled auto regressive auto regressive systems. *ISA Trans*, 91:99-113. https://doi.org/10.1016/j.isatra.2019.01.042

Mirjalili S, Lewis A., 2016. The Whale optimization algorithm. *Adv Eng Softw*, 95:51-67. https://doi.org/10.1016/j.advengsoft.2016.01.008

Mirjalili S, Mirjalili SM, Hatamlou A, 2016. Multi-verse optimizer: a nature-inspired algorithm for global optimization. *Neural Comput Appl*, 27(2):495-513. https://doi.org/10.1007/s00521-015-1870-7

Mishra BP, Panigrahi T, Wilson AM, et al., 2023. Nonlinear channel estimation based on robust distributed Hammerstein spline adaptive technique in wireless sensor network. *Digital Signal Process*, 132:103791. https://doi.org/10.1016/j.dsp.2022.103791

Nayak C, Saha SK, Kar R, et al., 2019. An efficient and robust digital fractional order differentiator based ECG pre-processor design for QRS detection. *IEEE Trans Biomed Circuits Syst*, 13(4):682-696. https://doi.org/10.1109/TBCAS.2019.2916676

Pal PS, Kar R, Mandal D, et al., 2017. Parametric identification with performance assessment of Wiener systems using brain storm optimization algorithm. *Circuits Syst Signal Process*, 36(8):3143-3181. https://doi.org/10.1007/s00034-016-0464-7

Patel V, Gandhi V, Heda S, et al., 2016. Design of adaptive exponential functional link network-based nonlinear filters. *IEEE Trans Circuits Syst I: Regul Pap*, 63(9):1434-1442. https://doi.org/10.1109/TCSI.2016.2572091

Raja MAZ, Aslam MS, Chaudhary NI, et al., 2018. Bio-inspired heuristics hybrid with interior-point method for active noise control systems without identification of secondary path. *Front Inf Technol Electron Eng*, 19(2):246-259. https://doi.org/10.1631/FITEE.1601028

Sankar S, Kar A, Burra S, et al., 2020. Nonlinear acoustic echo cancellation with kernelized adaptive filters. *Appl Acoust*, 166:107329. https://doi.org/10.1016/j.apacoust.2020.107329

Scarpiniti M, Comminiello D, Parisi R, et al., 2013. Nonlinear spline adaptive filtering. *Signal Process*, 93(4):772-783. https://doi.org/10.1016/j.sigpro.2012.09.021

Scarpiniti M, Comminiello D, Parisi R, et al., 2014. Hammerstein uniform cubic spline adaptive filters: learning and convergence properties. *Signal Process*, 100:112-123. https://doi.org/10.1016/j.sigpro.2014.01.019

Scarpiniti M, Comminiello D, Parisi R, et al., 2015a. Nonlinear system identification using IIR spline adaptive filters. *Signal Process*, 108:30-35. https://doi.org/10.1016/j.sigpro.2014.08.045

Scarpiniti M, Comminiello D, Parisi R, et al., 2015b. Novel cascade spline architectures for the identification of nonlinear systems. *IEEE Trans Circuits Syst I: Regul Pap*, 62(7):1825-1835. https://doi.org/10.1109/TCSI.2015.2423791

Scarpiniti M, Comminiello D, Parisi R, et al., 2018. Spline

Unedited

adaptive filters: theory and applications. In: Comminiello D, Príncipe JC (Eds.), Adaptive Learning Methods for Nonlinear System Modeling. Elsevier, Amsterdam, p.47-69. https://doi.org/10.1016/B978-0-12-812976-0.00004-X

Schetzen M, 1981. Nonlinear system modeling based on the Wiener theory. *Proc IEEE*, 69(12):1557-1573. https://doi.org/10.1109/PROC.1981.12201

Shadravan S, Naji HR, Bardsiri VK, 2019. The sailfish optimizer: a novel nature-inspired metaheuristic algorithm for solving constrained engineering optimization problems. *Eng Appl Artif Intell*, 80:20-34. https://doi.org/10.1016/j.engappai.2019.01.001

Shi YH, 2011. Brain storm optimization algorithm. Second Int Conf on Advances in Swarm Intelligence, p.303-309. https://doi.org/10.1007/978-3-642-21515-5_36

Storn R, Price K, 1997. Differential evolution - a simple and efficient heuristic for global optimization over continuous spaces. *J Glob Optim*, 11(4):341-359. https://doi.org/10.1023/A:1008202821328

Wang YJ, Tang SH, Gu XB, 2022. Parameter estimation for nonlinear Volterra systems by using the multi-innovation identification theory and tensor decomposition. *J Franklin Inst*, 359(2):1782-1802. https://doi.org/10.1016/j.jfranklin.2021.11.015

Wigren T, Schoukens J, 2013. Three free data sets for development and benchmarking in nonlinear system identification. European Control Conference (ECC), p.2933-2938. https://doi.org/10.23919/ECC.2013.6669201

Xu L, Jia HM, Lang CB, et al., 2019. A novel method for multilevel color image segmentation based on dragonfly algorithm and differential evolution. *IEEE Access*, 7:19502-19538. https://doi.org/10.1109/ACCESS.2019.2896673

Yadav S, Saha SK, Kar R, et al., 2022. EEG/ERP signal enhancement through an optimally tuned adaptive filter based on marine predators algorithm. *Biomed Signal Processd Control*, 73:103427. https://doi.org/10.1016/j.bspc.2021.103427

Yadav S, Saha SK, Kar R, 2023. An application of the Kalman filter for EEG/ERP signal enhancement with the autoregressive realisation. *Biomed Signal Process Control*, 86:105213. https://doi.org/10.1016/j.bspc.2023.105213

Yan H, Zhong CQ, Wu YH, et al., 2023. A hybrid-model optimization algorithm based on the Gaussian process and particle swarm optimisation for mixed-variable CNN hyperparameter automatic search. *Front Inf Technol Electron Eng*, 24(11):1557-1573. https://doi.org/10.1631/FITEE.2200515

Yang LD, Liu JX, Yan RQ, et al., 2019. Spline adaptive filter with arctangent-momentum strategy for nonlinear system identification. *Signal Process*, 164:99-109. https://doi.org/10.1016/j.sigpro.2019.06.007

Yu T, Li WQ, Yu Y, et al., 2021. Robust spline adaptive filtering based on accelerated gradient learning: design and performance analysis. *Signal Process*, 183:107965. https://doi.org/10.1016/j.sigpro.2021.107965

Yu T, Tan SJ, Li WQ, et al., 2024. Performance analysis of robust subband Hammerstein spline adaptive filter. *Circuits Syst Signal Process*, 43(1):368-387. https://doi.org/10.1007/s00034-023-02476-2

Zhang YF, Zhao ZD, Deng YJ, et al., 2021. ECGID: a human identification method based on adaptive particle swarm optimization and the bidirectional LSTM model. *Front Inf Technol Electron Eng*, 22(12):1641-1654. https://doi.org/10.1631/FITEE.2000511

The supplementary material consists of following sections:

1. A pictorial representation of the mathematical analysis HW-SAF modelling
2. The pseudocode of the proposed ROA-based CSAF design
3. Justification for the choice of common control parameters values
4. Parameter convergence profiles of Systems 2 using the ROA method
5. AE metric results for System 2 using the ROA, MVO, BSO and DE algorithms under different noise variance levels
6. Comparison of the performance of the techniques used for the System 2 design based on various performance indexes
7. Fitness convergence profiles for the System 2 design
8. Percentage improvement resulting from use of the proposed algorithm over others for System 1 and 2 designs
9. Statistical results of the estimated parameters of System 2
10. Statistical analysis of the global metric results for System 2
11. Fitness metric results from 100 independent runs of the algorithms used for System 2 design
12. Holm's consistency test
13. Proof of $O(MOA) = O(F(x)) \times O\left(NP \times \left(T\varpi + 1\right)\right)$
14. Basic details of the coupled electric drive system
15. The basic details of the CSTR system

Unedited